

Insignificant influence of the 11-year solar cycle on the North Atlantic Oscillation

Gabriel Chiodo ^{1*}, Jessica Oehrlein ¹, Lorenzo M. Polvani ^{1,2}, John C. Fyfe³ and Anne K. Smith ⁴

The North Atlantic Oscillation is the dominant mode of variability of atmospheric circulation outside of the tropics in the Northern Hemisphere in winter. To understand and attribute this mode of variability is of great societal relevance for populated regions in Eurasia. It has been widely claimed that there is a robust signal of the nearly periodic 11-year solar cycle in the North Atlantic Oscillation in winter, which thereby raises the possibility of using the solar cycle to predict the circulation years in advance. Here we present evidence that contradicts this claim. First, we show the absence of a solar signal in the North Atlantic Oscillation in the instrumental record prior to the mid-1960s, and a marginally significant signal thereafter. Second, from our analysis of a global chemistry–climate model repeatedly forced with the sequence of solar irradiance since the mid-1960s, we suggest that the solar signal over this period might have been a chance occurrence due to internal variability, and hence does not imply enhanced predictability.

Wintertime climate variability over the North Atlantic is substantially associated with the North Atlantic Oscillation (NAO), which is characterized by a sea level pressure (SLP) pattern with anomalies of one sign over Iceland and of the other over the subtropical Atlantic¹. Changes in the polarity of this pattern are associated with changes in the storm track, which in turn influence temperature and precipitation from the North Atlantic to central Eurasia². Several studies argue that the nearly periodic 11-year solar cycle can influence the NAO in winter^{3–7}. These studies suggest that during peaks in the sunspot cycle the NAO is more probably found in its positive polarity, with below (above) average SLP over Iceland (subtropical Atlantic). Most recently, it was reported that the NAO signal maximizes approximately 2–4 years after peaks in the sunspot cycle^{4,7}. Based on the proposed connection, mild and wet winters would be expected over much of Eurasia after a peak in the solar cycle. Given the regularity of the sunspot cycle, this would promise the real possibility of extended decadal predictability of the Northern Hemisphere climate^{3,8}. However, the robustness of the observed connection is unclear, and the mechanism whereby a small radiative forcing from the solar cycle ($\sim 0.2 \text{ W m}^{-2}$) causes a change in an index as noisy as the NAO remains elusive.

It is well established that an increased ultraviolet absorption around solar cycle maxima causes warming and increased ozone in the upper stratosphere⁹. Solar-induced changes in stratospheric temperatures produce circulation anomalies, which may induce a change in the polarity of the NAO via a ‘top-down’ mechanism^{3,10–12}. However, a lag of several years in the NAO response^{4,7} is difficult to reconcile with the fast timescale of stratosphere–troposphere coupling¹³. Some modelling evidence indicates a lagged response in the NAO^{5,6,14}. However, these studies are either based on simplified models forced with idealized step-like solar forcing perturbations⁵ or include both solar and other climate forcings, such as greenhouse gases (GHGs) and volcanic eruptions^{6,14}. Moreover, modelling studies that claim an apparent solar signal in the NAO are inconsistent in the estimated time lag between the solar maxima and NAO response, ranging from 0 years³, 1–2 years¹⁴ and up to 3–4 years^{5,6}.

Uncertainties also remain in the characterization of observed solar/NAO connections, as previous observational studies have only examined the solar signal in a single SLP reconstruction⁴. Such reconstructions typically assimilate a limited number of observations prior to 1950, and thus carry considerable uncertainty over the earlier periods. Correlations between solar variability and weather phenomena have long been proposed¹⁵, but many examples exist of solar connections being refuted on the basis of careful statistical analysis and/or additional observations^{16–18}. These challenges suggest the need to investigate the robustness of the proposed solar signal in the NAO.

The solar signal in the NAO in observations

We start by reproducing previous results^{4,7} using Hadley Center Sea Level Pressure version 2 (HadSLP) reconstructions of the North Atlantic SLP and expand on them by analysing additional data sets: National Center for Environmental Prediction Twentieth Century Reanalysis (20th Century), European Centre for Medium-Range Weather Forecasts 20th Century reconstruction (ERA20) and National Oceanic and Atmospheric Administration (NOAA) (Methods). We calculated the winter mean NAO index in these reconstructions and explored the statistical relationship between this index and the sunspot number (SSN), also referred to here as the solar index. Peaks in the NAO appear to coincide within a few years with peaks in the solar index over the later but not the earlier periods (Fig. 1a). To quantify this, we show in Fig. 1b the linear correlation between the NAO and the solar index over overlapping 40-year windows, shifted by 1 year at a time. Here, we lagged the solar index by two years, as this is the lag that gives the most robust SLP signal (Supplementary Figs. 1 and 2), consistent with previous results⁴. In all reconstructions, a lagged correlation is only seen in the later part of the record (after 1960). At its maximum ($r \approx 0.3$), the correlation implies that a small but important ($\sim 10\%$) fraction of the NAO variance might be explained by the solar cycle.

We then examined the pattern of the North Atlantic SLP associated with the solar index, taking into account several well-known

¹Department of Applied Physics and Applied Mathematics, Columbia University, New York, NY, USA. ²Lamont-Doherty Observatory, Columbia University, Palisades, NY, USA. ³Environment and Climate Change Canada, Victoria, British Columbia, Canada. ⁴National Center for Atmospheric Research, Boulder, CO, USA. *e-mail: chiodo@columbia.edu

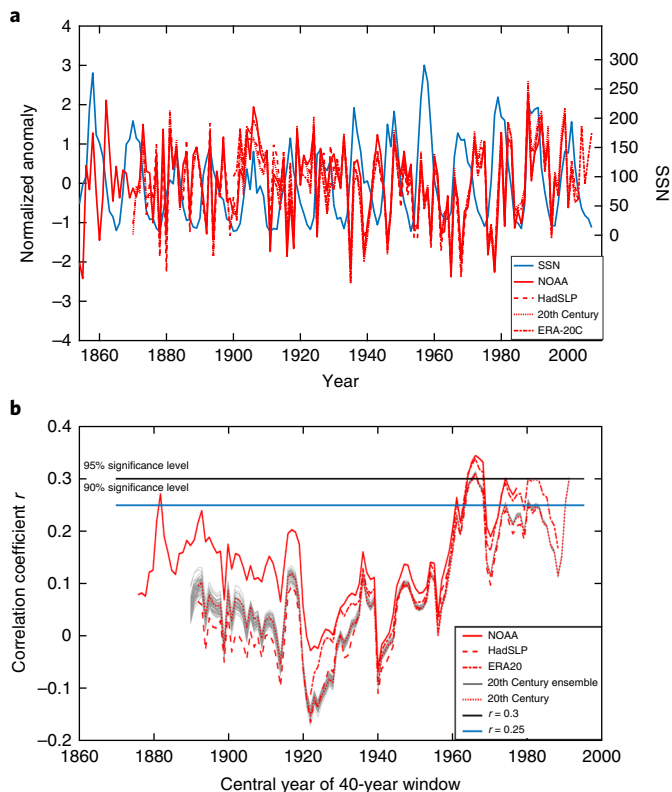


Fig. 1 | Statistical relationship between solar variability and the NAO index in observations. a, Time series of the SSN (blue) versus the NAO index calculated in four different reconstructions (red). **b**, The 40-year running mean correlation between SSN and the NAO at a lag of 2 years. The year on the x axis is the central year used in the 40-year windows. The grey shading represents the spread across individual 20th Century ensemble members. The blue and black horizontal bars denote the 90 and 95% significance levels (based on a Student *t*-test).

signals of climate variability. Specifically, over the full period covered by each reconstruction we performed a multiple linear regression between SLP and the solar index, the El Niño–Southern Oscillation (ENSO), aerosol optical depth (AOD), and a linear trend (Methods). We then analysed the spatial pattern of the regression coefficients associated with the lagged solar index, calculated by shifting the index one year at a time so that the SLP data lag the solar index, as done in other studies⁴⁷. Supplementary Figs. 1 and 2 show the pattern of the solar regression coefficient in each reconstruction as a function of the lag (in years) used in the solar index. We see the emergence of a pattern that consists of positive (negative) SLP anomalies in the south (north), a pattern typically associated with the positive NAO phase. This pattern is clearest at a lag of two years; this result is robust across all reconstructions when a common period is chosen across them (1901–1997 (Fig. 2)), which confirms the optimality of this lag in extracting a potential solar signal in the NAO. Even when using an ‘optimal’ time lag in the solar index, the solar regression coefficient is smaller than that associated with ENSO (Supplementary Fig. 3). Moreover, this pattern emerges in the later period (1958–1997) (Supplementary Fig. 4a–d)—consistent with Fig. 1b—but is not seen in other periods (1901–1940) (Supplementary Fig. 4e–h).

The overall pattern shown in Fig. 2 is suggestive of a possible solar signal in the NAO, but not conclusively so given the dependence of the signal on the analysis period. The relationship could be non-stationary, due to non-linear interactions with changes in the mean state¹⁹ or due to the amplitude of the sunspot cycle variability,

which appears to be larger in recent decades (Fig. 1a) and possibly results in a larger forcing of the NAO. An alternative explanation is that the solar signal is a manifestation of internal variability. To ascertain whether this pattern reflects a true solar signal, we turn to climate model simulations.

The solar signal in the NAO in models

We use the Community Earth System Model version 1.2, configured with the Whole Atmosphere Community Climate Model version 4 (WACCM) as its atmospheric component²⁰, coupled to ocean, sea-ice and interactive stratospheric ozone chemistry. This model simulates a realistic representation of shortwave heating and, consequently, of the upper atmospheric response to solar variability¹². We performed a 500-year long ocean-coupled integration, forced solely with a time-varying spectrally resolved solar forcing (hereafter referred to as WACCM SOL) to yield a total solar irradiance (TSI) of $1361.5 \pm 0.5 \text{ W m}^{-2}$. Solar variability in this integration is implemented by repeating 12 times, for each band of the solar spectrum, the sequence of the last four solar cycles (20–23) in the CMIP5 forcing data set²¹. These cycles are among the strongest on record, and produce the largest solar/NAO correlation (Fig. 1b). Moreover, the spectrally resolved solar flux over these cycles covers the satellite period, and is thus better constrained than over earlier cycles²². Most importantly, all non-solar forcings, such as GHGs and volcanic aerosols, are kept constant at year 2000 values to improve detection of the solar signal, unlike previous studies based on model simulations with time-varying solar and non-solar forcings^{4,6,14}. As a result of imposing constant GHG levels, our integration is in a steady state and can thus be used to study the solar/NAO connection in the absence of any mean state changes that could interfere in the detection of solar signals in the NAO.

The upper stratosphere is where the most robust solar signal is expected based on ultraviolet absorption by the ozone layer^{23–26}. Hence, we first focused on this region to validate the modelled atmospheric response to the solar cycle. To diagnose the solar signal in the observations, we regressed the upper stratospheric temperature data from the Stratospheric Sounding Unit (SSU)²⁷ and compared this regression against the output from the WACCM SOL simulation, interpolated onto the same SSU kernel (Methods). In the SSU, we found a statistically significant warming of 0.6 K (temperature change per solar cycle) in the tropics (Supplementary Fig. 5), in agreement with previous studies^{27,28}. The simulated and SSU values in this region are in excellent agreement, whereas in higher latitudes they lie within statistical uncertainty. The model also shows a stratospheric ozone increase of ~1–2% in the middle stratosphere at 1–10 hPa (Supplementary Fig. 6), in good agreement with observations²⁹. Averaged over 500 years, we found no evidence of a strengthening of the stratospheric polar vortex with peaks in the solar index, which may seem in contrast with National Centers for Environmental Prediction data for 1979–2008 (Supplementary Fig. 7). However, averaging over shorter (30 year) periods, we found that the model is not inconsistent with reanalysis (Supplementary Section B).

That our model captures the impact of solar variability on the chemical and thermal structure of the stratosphere increases our confidence in it as a tool for testing the hypothesis of a robust solar signal on the NAO. Thus, we analysed the relationship between a lagged solar index in the 500-year long model integration (TSI) and North Atlantic SLP. As our observational analysis, we performed a regression on all the available overlapping 100-year periods from the WACCM SOL simulation using a 2-year lag for the solar index, and contrasted these with the reconstructions (1901–1997). We can identify 100-year segments of the WACCM SOL simulation with SLP regression patterns that resemble those in observations (compare Figs. 2 and 3a). However, we can also identify other 100-year segments of the simulation with SLP patterns that are dissimilar (Supplementary Fig. 8a).

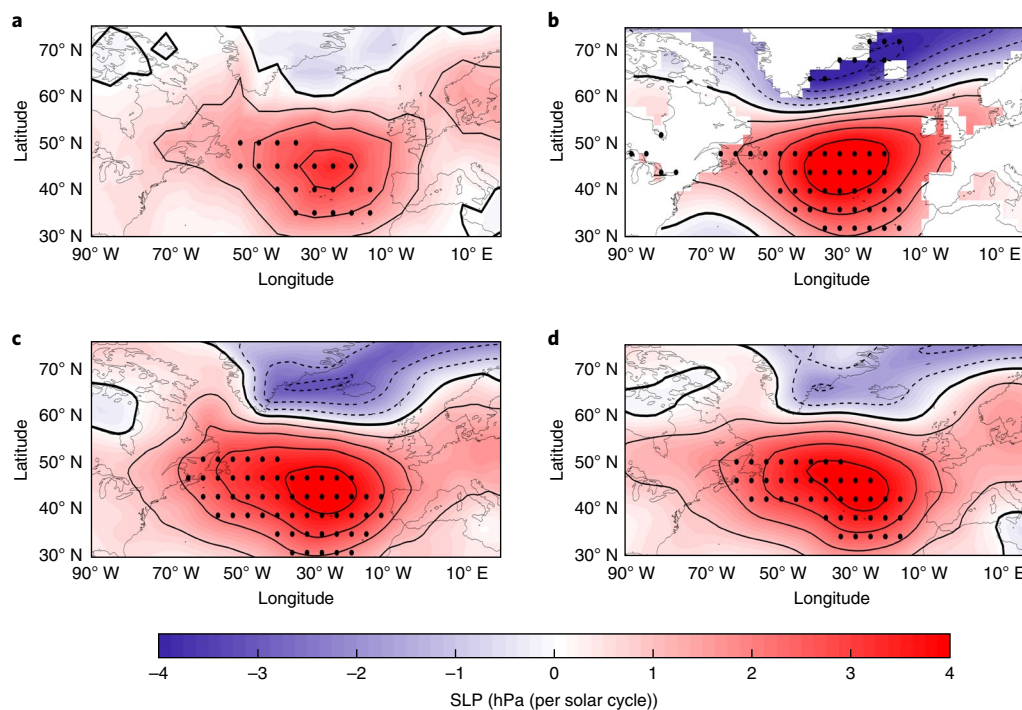


Fig. 2 | Lagged solar signal in reconstructions of the North Atlantic SLP. **a**, Solar regression coefficient for SLP from the HadSLP data set using a lag of 2 years (SSN leading SLP) over the period covered by the four reconstructions (that is, 1901–1997). **b–d**, As in **a** for NOAA (**b**), ERA20 (**c**) and 20th Century (**d**). Black dots represent statistically significant values at the 95% confidence level. Contour lines indicate 1 hPa increments.

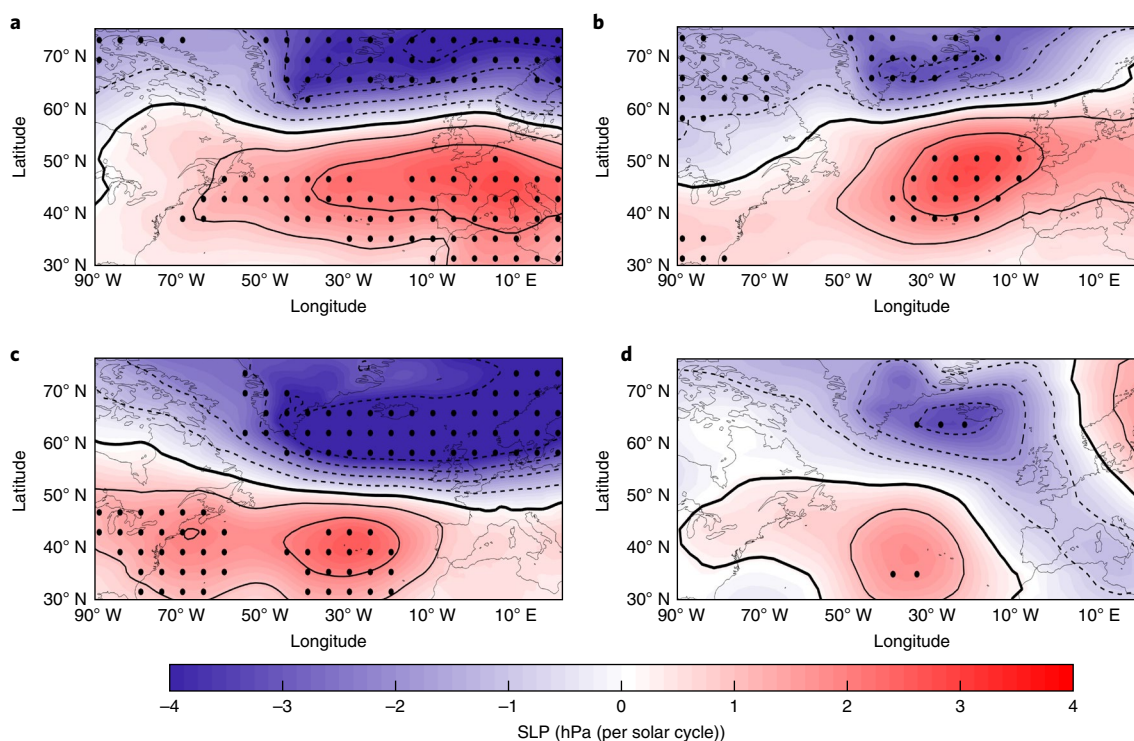


Fig. 3 | Lagged solar signal in the North Atlantic SLP from model simulations with and without a solar cycle. **a**, Solar regression coefficient in SLP, at a lag of 2 years (that is, TSI leading SLP) in a selected 100-year window in WACCM SOL (390–489). **b–d**, Same as in **a** for WACCM NOSOL (130–229) (**b**), LENS-CAM5 (801–900) (**c**) and CanESM2 (401–500) (**d**) (Methods selection criteria). Contour lines are 1 hPa increments.

This indicates that the SLP response is not robust across the 500 years of integration, although patterns that are similar to the observations can be found when using 100-year long records.

To gain further insight, we then turned our attention to another 500-year long WACCM simulation in which the solar flux was set to a constant value of $1,361.5 \text{ W m}^{-2}$ rather than varying in time—we

refer to this simulation as the WACCM NOSOL experiment. We computed the regression of North Atlantic SLP from this simulation with the 2-year lagged time-varying solar index. A time-varying solar index is inconsistent with the solar forcing imposed in this model integration and is deliberately used to determine whether the observed pattern in Fig. 2 might arise spontaneously from internal variability, without any influence by the 11-year solar cycle. Indeed, we can identify 100-year periods in WACCM NOSOL that exhibit SLP patterns which resemble the observed one (compare Figs. 2 and 3b). This finding weakens the suggestion that the observed pattern is a response to solar forcing and strengthens the case for internal variability.

To verify this result in other models, we analysed simulations from two large initial-condition ensemble experiments, performed with the Community Atmosphere Model version 5 (LENS-CAM5)³⁰ and the Canadian Earth System Model version 2 (CanESM2)³¹. Both simulations are 1,000 years long with a constant TSI of $1,361.5 \text{ W m}^{-2}$. As in WACCM NOSOL, we found 100-year segments in which the overall SLP patterns are similar to observations (compare Fig. 2 with Fig. 3c,d). Again, we found other 100-year segments in which this is not the case (Supplementary Fig. 8c,d). These findings bring into question the assertion that the NAO is robustly influenced by solar variability. To gain conclusive insight into the role of internal variability, we next quantified the likelihood of detecting the observed solar/NAO signal.

Probability of a solar cycle connection

We first extracted the solar signal in the NAO index, by regressing the latter against a lagged solar index, ENSO, AOD and linear trend. In this calculation, the solar/NAO signal is the regression coefficient associated with the 2-year lagged solar index, measured in units of standard deviations of the NAO per solar cycle variation. The solar/NAO signal in SLP reconstructions evaluated over 1958–1997 (covering cycles 20–23) is 0.80 ± 0.11 , using 95% confidence intervals on the reconstruction average (Fig. 4a). The WACCM SOL simulation is based on 12 repetitions of solar cycles 20–23 (black dots in Fig. 4a): from these we obtain a mean solar/NAO signal of 0.24 ± 0.26 , where confidence intervals are on the mean evaluated at the 95% confidence level (red bar in Fig. 4a). The 5–95% range of coefficients is 0.24 ± 0.70 . In words, (1) we did not find a robust solar signal and (2) the observed signal, although statistically significant, is within the range of internal variability simulated in the model.

We then considered the distribution of solar/NAO signals in the WACCM NOSOL simulation, recalling that the solar flux is kept constant here so that any solar/NAO linkage arises by chance. We considered all the overlapping 40-year segments (equivalent to 1958–1997). The histogram of the solar regression coefficient in the NAO is shown in Fig. 4a. The observed signals over the recent past decades fall within the distribution and are at the ~87th percentile of the simulated signals in WACCM NOSOL, the latter being due to internal variability alone. A similar conclusion is drawn from LENS-CAM5 and CanESM2 (Supplementary Fig. 9a,c). Although the observed signals are at the upper end of the simulated values, they cannot be statistically distinguished from internal variability, as the odds of finding a signal that exceeds the observed value in unforced model simulations are generally higher than 10%.

This conclusion is strengthened by using a longer 97-year period (1901–1997) (Fig. 4b and Supplementary Fig. 9b,d)—the observed signals then fall within the ~80th percentile of the unforced model simulations. Thus, internal variability appears capable of generating decadal signals in the NAO that can erroneously be attributed to the solar cycle in the observational record.

The NAO index is a complex time series that consists of superimposed fluctuations across a broad spectrum of frequencies³². To isolate NAO variations in the range of frequencies associated with the solar cycle, Thiéblemont et al.¹⁴ applied a band-pass filter to

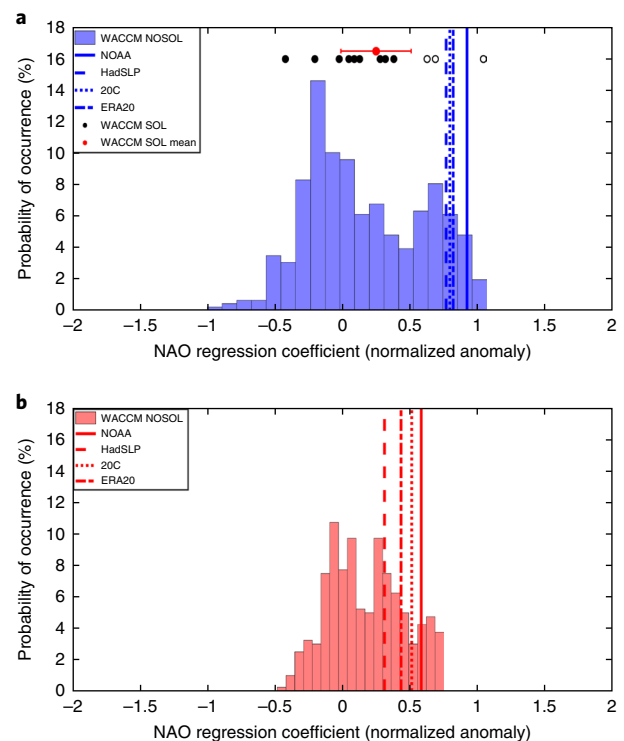


Fig. 4 | Distribution of the NAO solar regression coefficient in observations and models. **a**, Histogram of the solar regression coefficient on overlapping 40-year segments in WACCM NOSOL. Open (filled) black dots represent coefficients obtained in 12 non-overlapping 40-year segments for WACCM SOL, which are significant (not significant) at the 95% level; the red dot represents their average, with the s.e.m. Vertical bars show the coefficients from the reconstructions over 1958–1997. **b**, As **a**, but for 97-year overlapping segments in WACCM NOSOL (1901–1997 for the reconstructions). The regression coefficients from reconstructions over 1958–1997 (1901–1997) are located at the 85–89th (67–89th) percentile of the 40-year (97-year) WACCM NOSOL distribution.

exclude variations outside the range of 9–13 years. In a 150-year long WACCM simulation employing time-varying irradiance they found some phasing between the simulated band-pass filtered NAO index and the solar index. In contrast, in a 150-year simulation with constant irradiance they found no such coherence. From this, they concluded that quasi-decadal variations in the NAO index may have some degree of ‘synchronization’ with the solar cycle. Nevertheless, the synchronization seen in Thiéblemont et al.¹⁴ is far from perfect—peaks and valleys in their simulated band-pass filtered NAO index line up with the peaks and valleys in the solar index in some but not in all periods. This is analogous to what we have shown above in the unfiltered NAO index in observations and simulations, and once again, raises the issue of robustness.

We explored the synchronization hypothesis¹⁴ by analysing our longer WACCM simulations (500-year as compared to 150-year in Thiéblemont et al.¹⁴) and a wavelet analysis, which allowed us to investigate the time evolution of the NAO frequency spectrum without tampering with its integrity through filtering. Figure 5a shows that in SLP reconstructions (for simplicity, we only show HadSLP), there is an enhanced spectral power on interannual (3–5 years), quasi-decadal (7–9 years) and multi-decadal (20–25 years) timescales, in agreement with other studies^{32–34}. Spectral peaks in these frequencies come and go over time^{32,35}. During the times of increased variance in any of these frequencies, there is overlap between these spectral peaks and the 10–12-year frequency,

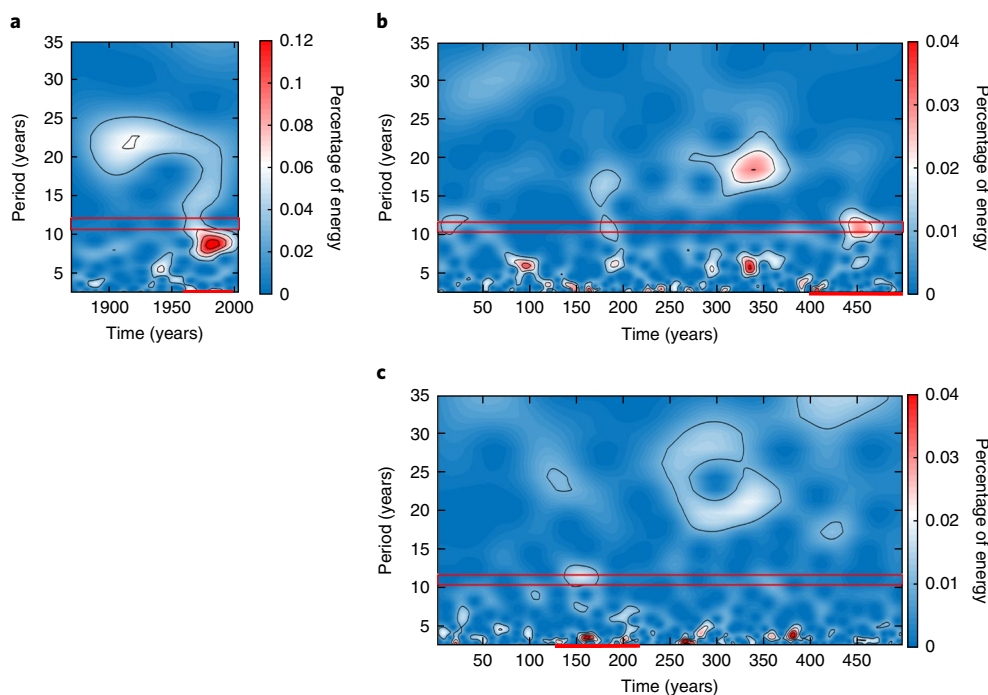


Fig. 5 | Time-frequency analysis of the NAO index. **a**, Spectral power as a function of time and frequency for the NAO index calculated from the HadSLP reconstruction. The red box identifies the frequency range in which solar irradiance exhibits the most prominent spectral peak (10–12 years). **b, c**, As in **a** for WACCM SOL (**b**) and for WACCM NOSOL (**c**). Red lines along the x axis identify the periods over which a strong solar/NAO signal is extracted using regression analysis in each respective data set.

characteristic of the sunspot cycle. As a result, decadal oscillations can map onto the sunspot cycle frequency: this is seen, for example, around 1970–1980 in HadSLP (Fig. 5a), and is consistent with the larger solar/NAO correlation obtained in this period (Fig. 1b). WACCM reproduces these sporadic appearances at the 10–12 year frequency, irrespective of the presence of a solar cycle forcing. Compare, for instance, the wavelet analysis in WACCM SOL and WACCM NOSOL in Fig. 5b,c. These periods of enhanced power at decadal timescales are consistent with the location of 100-year long segments, over which a significant solar/NAO signal is seen (that is, years 390–489 in WACCM SOL and years 130–229 in WACCM NOSOL (Fig. 3a,b)). Overall, the presence of a solar cycle only slightly enhances power at decadal frequencies, but this is not significant over the 500-year period (Supplementary Fig. 10). Hence, quasi-decadal variations in the NAO, such as those attributed to the solar variability, can arise due to internal variability alone.

Implications for predictability

Our results clearly show that quasi-decadal (11-year) variations in the North Atlantic SLP, such as those commonly attributed to solar variability, can be a manifestation of internal variability. Variability of the NAO at decadal timescales can arise naturally, without external drivers other than ocean–atmosphere coupling. Using long coupled model simulations forced with a realistic solar cycle variability, we show here that the forced response of the NAO is weak compared to the range of internal variability. Using 12 repetitions of solar cycles 20–23, we obtained a standard deviation (the ‘noise’) of ~ 0.40 and an average (the ‘signal’) of 0.24, that is a signal-to-noise ratio of ~ 0.6 . Hence, the prediction skill in winter circulation over the North Atlantic may not be significantly enhanced by including solar forcing. These results are in contrast with recent modelling studies that suggest a robust solar link in the NAO^{3,5,14}; possible reasons for the disagreement are the more realistic solar forcing and the longer simulations considered here. In support of this explanation,

we found that one needs an unrealistically large forcing to obtain a significant ‘top-down’ influence on the NAO in our model (Supplementary Section C).

Our results are consistent with the negligible role of solar variability in NAO reconstructions over the past millennium³⁶, and the non-stationarity of the statistical link between the solar cycle and the NAO in the twentieth century (Fig. 1b). Several caveats might affect our conclusions. First, the lack of a solar signal in the NAO in the early part of the 20th century could be due to the scarcity of observations prior to 1950. Second, the predictable component of the NAO in the current generation of climate models appears to be sometimes lower than observations³⁷. Hence, the modelled NAO may not be sufficiently sensitive to external forcings, which include the solar cycle. In spite of these caveats, our results call for caution against interpreting quasi-decadal signals in the relatively short observational record. Longer records are needed for an improved characterization of a forced response and internal variability in the mid-latitude wintertime circulation.

Online content

Any methods, additional references, Nature Research reporting summaries, source data, statements of data availability and associated accession codes are available at <https://doi.org/10.1038/s41561-018-0293-3>.

Received: 24 June 2018; Accepted: 17 December 2018;

Published online: 21 January 2019

References

1. Barnston, A. G. & Livezey, R. E. Classification, seasonality and persistence of low-frequency atmospheric circulation patterns. *Mon. Weather Rev.* **115**, 1083–1126 (1987).
2. Hurrell, J. W. Decadal trends in the North Atlantic Oscillation: regional temperatures and precipitation. *Science* **269**, 676–679 (1995).

3. Ineson, S. et al. Solar forcing of winter climate variability in the Northern Hemisphere. *Nat. Geosci.* **4**, 753–757 (2011).
4. Gray, L. J. et al. A lagged response to the 11 year solar cycle in observed winter Atlantic/European weather patterns. *J. Geophys. Res.* **118**, 13405–13420 (2013).
5. Scaife, A. A. et al. A mechanism for lagged North Atlantic climate response to solar variability. *Geophys. Res. Lett.* **40**, 434–439 (2013).
6. Andrews, M., Knight, J. & Gray, L. A simulated lagged response of the North Atlantic Oscillation to the solar cycle over the period 1960–2009. *Env. Res. Lett.* **10**, L054022 (2015).
7. Gray, L., Woollings, T., Andrews, M. & Knight, J. Eleven-year solar cycle signal in the NAO and Atlantic/European blocking. *Q. J. R. Meteorol. Soc.* **142**, 1890–1903 (2016).
8. Scaife, A. et al. Skillful long-range prediction of European and North American winters. *Geophys. Res. Lett.* **41**, 2514–2519 (2014).
9. Haigh, J. D. The impact of solar variability on climate. *Science* **272**, 981–984 (1996).
10. Kodera, K. & Kuroda, Y. Dynamical response to the solar cycle. *J. Geophys. Res.* **107**, 4749 (2002).
11. Matthes, K., Kuroda, Y., Kodera, K. & Langematz, U. Transfer of the solar signal from the stratosphere to the troposphere: northern winter. *J. Geophys. Res.* **111**, D06108 (2006).
12. Chiodo, G., Calvo, N., Marsh, D. & Garcia-Herrera, R. The 11 year solar cycle signal in transient simulations from the whole atmosphere community climate model. *J. Geophys. Res.* **117**, D06109 (2012).
13. Gerber, E. P. & Polvani, L. M. Stratosphere–troposphere coupling in a relatively simple AGCM: the importance of stratospheric variability. *J. Clim.* **22**, 1920–1933 (2009).
14. Thiéblemont, R., Matthes, K., Omrani, N.-E., Kodera, K. & Hansen, F. Solar forcing synchronizes decadal North Atlantic climate variability. *Nat. Commun.* **6**, 8268 (2015).
15. Siscoe, G. L. Solar-terrestrial influences on weather and climate. *Nature* **276**, 348–352 (1978).
16. Baldwin, M. & Dunkerton, T. Observations and statistical simulations of a proposed solar cycle/QBO/weather relationship. *Geophys. Res. Lett.* **16**, 863–866 (1989).
17. Pittock, B. Can solar variations explain variations in the Earth's climate? *Clim. Change* **96**, 483–487 (2009).
18. Turner, T. E. et al. Solar cycles or random processes? Evaluating solar variability in Holocene climate records. *Sci. Rep.* **6**, 23961 (2016).
19. Van Loon, H. & Meehl, G. A. Interactions between externally forced climate signals from sunspot peaks and the internally generated Pacific Decadal and North Atlantic Oscillations. *Geophys. Res. Lett.* **41**, 161–166 (2014).
20. Marsh, D. R. et al. Climate change from 1850 to 2005 simulated in CESM1 (WACCM). *J. Clim.* **26**, 7372–7391 (2013).
21. Wang, Y.-M., Lean, J. & Sheeley, N. Modeling the Sun's magnetic field and irradiance since 1713. *Astrophys. J.* **625**, 522–538 (2005).
22. Ermolli, I. et al. Recent variability of the solar spectral irradiance and its impact on climate modelling. *Atmos. Chem. Phys.* **13**, 3945–3977 (2013).
23. Crooks, S. & Gray, L. Characterization of the 11-year solar signal using a multiple regression analysis of the ERA-40 dataset. *J. Clim.* **18**, 996–1015 (2005).
24. Frame, T. & Gray, L. J. The 11-year solar cycle in ERA-40 data: an update to 2008. *J. Clim.* **23**, 2213–2222 (2010).
25. Chiodo, G., Marsh, D., Garcia-Herrera, R., Calvo, N. & Garca, J. On the detection of the solar signal in the tropical stratosphere. *Atmos. Chem. Phys.* **14**, 5251–5269 (2014).
26. Mitchell, D. et al. Signatures of naturally induced variability in the atmosphere using multiple reanalysis datasets. *Q. J. R. Meteorol. Soc.* **141**, 2011–2031 (2014).
27. Seidel, D. J. et al. Stratospheric temperature changes during the satellite era. *J. Geophys. Res.* **121**, 664–681 (2016).
28. Randel, W. J., Smith, A. K., Wu, F., Zou, C. Z. & Qian, H. Stratospheric temperature trends over 1979–2015 derived from combined SSU, MLS, and SABER satellite observations. *J. Clim.* **29**, 4843–4859 (2016).
29. Maycock, A., Matthes, K., Tegtmeier, S., Thiéblemont, R. & Hood, L. The representation of solar cycle signals in stratospheric ozone—part 1: a comparison of recently updated satellite observations. *Atmos. Chem Phys.* **16**, 10021–10043 (2016).
30. Kay, J. et al. The Community Earth System Model (CESM) large ensemble project: a community resource for studying climate change in the presence of internal climate variability. *Bull. Am. Meteorol. Soc.* **96**, 1333–1349 (2015).
31. von Salzen, K. et al. The Canadian fourth generation atmospheric global climate model (CanAM4). Part I: representation of physical processes. *Atmos. Ocean* **51**, 104–125 (2013).
32. Hurrell, J. W., Kushnir, Y., Ottersen, G. & Visbeck, M. in *The North Atlantic Oscillation: Climatic Significance and Environmental Impact* (ed. Lifland, J.) 1–35 (American Geophysical Union, 2003).
33. Hurrell, J. W. & Van Loon, H. in *Climate Change at High Elevation Sites* (eds Diaz, H. F., Beniston, M. & Bradley, R. S.) 69–94 (Springer, Berlin, 1997).
34. Wang, X., Li, J., Sun, C. & Liu, T. NAO and its relationship with the Northern Hemisphere mean surface temperature in CMIP5 simulations. *J. Geophys. Res.* **122**, 4202–4227 (2017).
35. Wanner, H. et al. North Atlantic Oscillation—concepts and studies. *Surv. Geophys.* **22**, 321–381 (2001).
36. Ortega, P. et al. A model-tested North Atlantic Oscillation reconstruction for the past millennium. *Nature* **523**, 71–74 (2015).
37. Smith, D. M., Scaife, A. A., Eade, R. & Knight, J. R. Seasonal to decadal prediction of the winter North Atlantic Oscillation: emerging capability and future prospects. *Q. J. R. Meteorol. Soc.* **142**, 611–617 (2016).

Acknowledgements

This work is supported by a grant from the US National Science Foundation (NSF) and a cooperative agreement between NASA and Columbia University. J.O. is funded by the NSF grant DGE 1644869. All model integrations were performed at the National Center for Atmospheric Research, which is sponsored by the US NSF. The authors thank M. Sigmund and N. Gillett (Canadian Centre for Climate Modelling and Analysis) for helpful comments. We acknowledge Environment and Climate Change Canada's Canadian Centre for Climate Modelling and Analysis for executing and making available the CanESM2 large ensemble simulations, and the Canadian Sea Ice and Snow Evolution (CanSISE) Network for proposing the simulations.

Author contributions

G.C. ran the climate model experiments and wrote the paper, J.O. performed the analysis of the observational and model data and G.C., J.O., L.M.P., J.C.F. and A.K.S. designed the research. All the authors helped in discussing ideas, interpreting results and writing the paper.

Competing interests

The authors declare no competing interests.

Additional information

Supplementary information is available for this paper at <https://doi.org/10.1038/s41561-018-0293-3>.

Reprints and permissions information is available at www.nature.com/reprints.

Correspondence and requests for materials should be addressed to G.C.

Publisher's note: Springer Nature remains neutral with regard to jurisdictional claims in published maps and institutional affiliations.

© The Author(s), under exclusive licence to Springer Nature Limited 2019

Methods

Observational data sets. To analyse the solar signal in the North Atlantic boreal winter SLP fields, we used winter mean (December–January–February (DJF) average) SLP data from four reconstructions: HadSLP³⁸, 20th Century³⁹, ERA20⁴⁰ and the Extended Reconstructed SLP data set from the NOAA⁴¹. HadSLP is on a 5° latitude times 5° longitude global grid, and covers the 1860–2007 period³⁸. The 20th Century Re-analysis V2 SLP is on a 5° grid, and provides 55 individual members (using different initial conditions) covering the period 1872–2014³⁹. The NOAA Extended Reconstructed SLP has a 2° resolution, and covers the 1852–1998 period⁴¹: this data set only provides SLP over the ocean. Finally, the ERA20 data set is on a 1° global grid and covers the 1900–2010 period. For practical purposes, we used the reconstructed data in their native grid resolution (hence, the land portion of the NOAA data is masked out) and considered both the full available period covered by each reconstruction (for example, Supplementary Fig. 1) as well as the common period (1901–1997).

These products provide a comprehensive global atmospheric circulation data set that spans the twentieth century. Prior to the satellite and radiosonde era (that is, before 1950), they mostly assimilate surface pressure and surface marine wind observations taken from the International Comprehensive Ocean–Atmosphere Data Set and land observations from available stations around the globe. Despite similarities in their sources of data, these products employ different assimilation schemes and numerical models, and can thus be deemed as four independent observational data sets.

Models. The WACCM model is coupled to the Parallel Ocean Program ocean circulation model. This model employs a nominal latitude–longitude resolution of 1° (down to 1/4° in latitude in the equatorial tropics)⁴². The resolution in WACCM is 1.9° latitude and 2.5° longitude with 66 vertical levels and an upper boundary at 140 km, which provides a well-resolved middle atmosphere. The standard configuration of WACCM includes a fully interactive stratospheric chemistry module, which calculates more than 100 gas-phase chemical reactions and the advection of chemical species⁴³. Most importantly, stratospheric ozone is fully interactive. Photolysis rates are calculated in-line using a resolution of 66 bands that covers all absorption lines from 120 nm onwards⁴⁴.

Experiment design. We performed two 500-year long ocean-coupled integrations from WACCM, using a constant year 2000 boundary condition: one integration with a time-varying irradiance forcing (WACCM SOL), and one with a constant irradiance forcing (WACCM NOSOL). In WACCM SOL, we repeated the sequence of the last four sunspot cycles on record (that is cycles 20, 21, 22 and 23) throughout the 500 year integration. The spectral solar irradiance forcing and its variability are taken from Wang et al.²¹, consistent with the solar forcing employed in historical integrations from CMIP5⁴⁵. To create a spectrally resolved 500-year long solar forcing record for the WACCM SOL integration, we took the sequence of solar cycles 20–23 for each individual spectral band from 121 to 1,500 nm from Wang et al.²¹, and repeated such a sequence 12 times. In WACCM NOSOL, we used an average spectral solar irradiance forcing averaged over the last four cycles, and the resulting TSI is 1,361.5 W m⁻². Other forcings, such as GHGs and ODSs, were set at year 2000 values. To isolate the effects of solar irradiance, we excluded energetic particle forcing. To include a representation of the quasi-biennial oscillation in stratospheric winds, we included a periodic (28 months) quasi-biennial oscillation forcing in all the integrations⁴⁶.

To assess the range of internal variability in the North Atlantic SLP, irrespective of the presence of the 11-year solar cycle, we also complemented the WACCM runs with 1,000-year long pre-industrial integrations from two other models and imposed a constant TSI forcing. More specifically, we used one CAM5 integration from the ‘Large Ensemble’³⁰ and one CanESM2 run³¹. Both runs thus mimic the set-up of WACCM NOSOL, except for the boundary conditions, which are set at 1850.

Stratospheric temperature data. To analyse the observed solar signal in the upper stratospheric temperature and validate models, studies have typically employed reanalysis data sets that span the satellite period (1979 to present)^{12,47}. However, it has been shown that in the upper stratosphere these products suffer from abrupt jumps when observational data from new satellite instruments are introduced. Moreover, they are poorly constrained, as radiosonde observations are not available in this atmospheric region. Both issues lead to a possible overestimate of the equatorial upper stratospheric solar signal in reanalysis²⁶, which limits the usefulness of these products for the validation of models and their ability to capture the atmospheric response to solar variability. To overcome these issues, we validated the solar response in WACCM SOL against data from the SSU²⁷. For the models and SSU comparison (Supplementary Fig. 5a), we examined the period covered by SSU from 1979 to 2016. Specifically, we used data from Channel 3 of the SSU, which has a weighting function that peaks at around 50 km, which provides an estimate of the upper stratospheric temperature. To directly compare the satellite data and model output, we applied the same SSU kernel function on atmospheric temperature to the WACCM SOL simulation output, taken from the full 500-year long simulated period. Then, we extracted the observed and

simulated solar signals via regression, with TSI as the predictor instead of SSN, to be consistent with the actual forcing imposed in WACCM SOL.

Statistical analysis. The NAO is calculated by using principle component analysis (PCA), following the definition proposed in the literature⁴⁸. More specifically, we took the first principal component and analysed its deseasonalized anomalies for the DJF season. Anomalies were taken against the mean of the entire data series. The 11-year solar signal in the DJF mean SLP, and stratospheric temperature was extracted by means of multiple linear regression analysis using predictors that are consistent with the boundary conditions of the pertaining data set. Hence, in observations we used the SSN available at www.sidc.be/silo/datafiles, the observed NINO3.4 index (www.esrl.noaa.gov/psd/gcos_wgsp/Timeseries/Data/nino34.longanom.data), an AOD index (<https://data.giss.nasa.gov/modelforce/strat aer/>) and a linear term.

Following the analysis method in ref. 4, the solar regression coefficient in reconstructed SLP data is obtained by regressing de-seasonalized DJF mean SLP (in hPa) onto standardized anomalies of the SSN index, as well as the ENSO; reflecting teleconnected variability from the tropical Pacific), 3) stratospheric aerosol (AOD; representing volcanic influences) and 4) a term that is linear in time (representing combined anthropogenic influences). The lagged solar regressions are then calculated by shifting the index one year at a time so that the SLP data lag the solar index, with all other indices kept at zero lag, following Gray et al.⁴⁷. Then, we multiplied the regression coefficient by the maximum peak-to-trough variation (in s.d. units) of the SSN to obtain an estimate of the maximum likely response of SLP (hPa) to variations in the Sun’s output. This same procedure was repeated for the regression of SLP data from the models, using TSI as a predictor instead of the SSN, to be consistent with the actual forcing imposed in the model. In practice, DJF mean values of SSN and TSI were highly correlated (0.97), so the results are not sensitive to the choice of the solar index in the observational analysis. For the model results, we specifically chose 100-year periods, because this is close to the length of the common period covered by all four reanalysis data sets (1901–1997; that is, 97 years). The simulation periods shown in Fig. 3 were selected by calculating the running-mean correlation of the NAO index and TSI, and finding the peaks in such correlations. The statistical significance of all the regression coefficients was assessed by using a two-sided Student’s *t*-test, including an AR-1 correction in the confidence intervals^{24,49}.

Calculation of NAO distributions in unforced model simulations. For the calculation of the histograms of the solar regression in the NAO in simulations without a solar cycle forcing, we considered all the maximally overlapping (shifted by 1 year at a time) periods of length equivalent to the period that spanned solar cycles 20–23 (40 years), and used the observed (time-varying) 2-year lagged solar index in the regression of the NAO from WACCM SOL, LENS-CAM5 and CanESM2. The procedure was repeated on 40-year (97-year) periods, for comparison with the short (1958–1997) and full (1901–1997) common period across the four reconstructions.

Spectral analysis of the NAO. Finally, we performed time-frequency and spectrum analyses of the calculated NAO index from the reconstructions and the WACCM simulations by using the continuous wavelet toolbox available in Matlab (www.mathworks.com/products/wavelet.html) as well as the multitaper power spectral density (www.mathworks.com/help/signal/ref/pmtm.html).

Code availability

The source code of the WACCM model is part of the Community Earth System Model version 1.2.0, which is publicly distributed and can be obtained after registration at www.cesm.ucar.edu/models/cesm1.2/. All the figures were produced with Matlab, version R2017a, available at www.mathworks.com. The algorithm used to perform regression, PCA and wavelet analysis was written using built-in functions from the same Matlab distribution. More specifically, regression analysis is based on the `regstats` function (www.mathworks.com/help/stats/regstats.html), the wavelets on the `CWT` function (www.mathworks.com/help/wavelet/ref/cwt.html) and the PCA on the `SVD` function (www.mathworks.com/help/matlab/ref/svd.html).

Data availability

HadSLP, NOAA and 20th Century reconstructions data were provided by the NOAA/OAR/ESRL PSD from their website at www.esrl.noaa.gov/psd/. ERA20 data were archived by ECMWF from their website at www.ecmwf.int/en/forecasts/datasets/archive-datasets/reanalysis-datasets/era-20c. The SSU data are available at www.remss.com/measurements/upper-air-temperature/. The CanESM2 model data are available at <http://climate-modelling.canada.ca/climatemodeldata/cgcm4/CanESM2/esmControl/index.shtml>. The LENS-CAM5 model data are available through the Climate Data Gateway, hosted at NCAR and are accessible at www.earthsystemgrid.org/dataset/ucar.cgd.cesm4.output.html. Finally, the WACCM model data are stored and available in the HPSS archive on the NCAR’s Computational and Information Systems Lab, located at www2.cisl.ucar.edu/resources/storage-and-file-systems/hpss/access.

References

38. Allan, R. & Ansell, T. A new globally complete monthly historical gridded mean sea level pressure dataset (HadSLP2): 1850–2004. *J. Clim.* **19**, 5816–5842 (2006).
39. Compo, G. P. et al. The twentieth century reanalysis project. *Q. J. R. Met. Soc.* **137**, 1–28 (2011).
40. Poli, P. et al. *The Data Assimilation System and Initial Performance Evaluation of the ECMWF Pilot Reanalysis of the 20th-Century Assimilating Surface Observations Only (ERA-20C)* ERA Report Series No. 14 (ECMWF, 2013).
41. Smith, T. M. & Reynolds, R. W. Reconstruction of monthly mean oceanic sea level pressure based on COADS and station data (1854–1997). *J. Atmos. Ocean Tech.* **21**, 1272–1282 (2004).
42. Gent, P. R. et al. The Community Climate System Model version 4. *J. Clim.* **24**, 4973–4991 (2011).
43. Kinnison, D. et al. Sensitivity of chemical tracers to meteorological parameters in the MOZART-3 chemical transport model. *J. Geophys. Res.* **112**, D20302 (2007).
44. Marsh, D. et al. Modeling the whole atmosphere response to solar cycle changes in radiative and geomagnetic forcing. *J. Geophys. Res.* **112**, D23306 (2007).
45. Taylor, K. E., Stouffer, R. J. & Meehl, G. A. An overview of CMIP5 and the experiment design. *Bull. Am. Meteorol. Soc.* **93**, 485–498 (2012).
46. Matthes, K. et al. Role of the QBO in modulating the influence of the 11 year solar cycle on the atmosphere using constant forcings. *J. Geophys. Res.* **115**, D18110 (2010).
47. Mitchell, D. et al. Solar signals in CMIP-5 simulations: the stratospheric pathway. *Q. J. R. Meteorol. Soc.* **141**, 2390–2403 (2015).
48. Hurrell, J. W. & Deser, C. North Atlantic climate variability: the role of the North Atlantic Oscillation. *J. Marine Syst.* **79**, 231–244 (2010).
49. Tiao, G. et al. Effects of autocorrelation and temporal sampling schemes on estimates of trend and spatial correlation. *J. Geophys. Res.* **95**, 20507–20517 (1990).